THE CALIF^{3}S-P^{2}REMICS SOFTWARE – AN APPLICATION TO UNDEREXPANDED HYDROGEN JET DEFLAGRATION

L. Gastaldo

Institut de Radioprotection et de Sûreté Nucléaire (IRSN)
St Paul-Lez-Durance, 13115, France
laura.gastaldo@irsn.fr

ABSTRACT

To assess explosion hazard, the french Institut de Radioprotection et de Sûreté Nucléaire (IRSN) is developping the P^{2}REMICS software (for Partially PREMIxed Combustion Solver) on the basis of the generic CFD solver library CALIF^{3}S (for Components Adaptive Library for Fluid Flow Simulation). Both P^{2}REMICS and CALIF^{3}S are in-house IRSN softwares, released under an open-source license. CALIF^{3}S-P^{2}REMICS is dedicated to the simulation of explosion scenarii (explosive atmosphere formation, deflagration or detonation and blast waves propagation), for hydrogen as, more generally, for any explosive gas or gas/dust mixture. It is based on staggered space discretizations and implements fractional-steps time algorithms, well suited for massively parallel computations. A wide range of experiments is used for the software validation. Among them, we focus here on a free underexpanded hydrogen jet deflagration, performed in two steps: first, the hydrogen is released in air, up to obtain a steady jet (dispersion phase), then the deflagration is triggered. For the dispersion phase simulation, a notional nozzle approach is used to get rid of the description of the shocked zone located near the nozzle. Then a so-called turbulent flame velocity approach is chosen for the deflagration simulation. The computations allow to highlight the complex flow structures induced by the inhomogeneity fuel concentration in the jet. A large dispersion of results is observed, depending on the chosen correlation for the turbulent flame speed.

1.0 INTRODUCTION

Accelerated turbulent deflagrations, potentially transiting to detonation, are a major hazard in industrial plants, and more specially in nuclear power plants. The French Institut de Radioprotection et de Sûreté Nucléaire (IRSN) has the aim to enhance its capability of predictive risk evaluation in this field. Thus, IRSN is developing a simulation tool, named P^{2}REMICS (for Partially PREMIxed Combustion Solver), to compute the formation of explosive atmospheres, their deflagration or detonation and the subsequent propagation of blast waves. The P^{2}REMICS [1] software is built as a specific application of the generic CFD solver library CALIF^{3}S [2] (for Components Adaptative Library For Fluid Flow Simulations), which deals with a wide range of applications, including laminar and turbulent flows, potentially reactive, governed by incompressible, low Mach number or compressible Navier-Stokes equations. Both P^{2}REMICS and CALIF^{3}S are available free softwares, respectively under the CeCILL V2 and the CeCILL-C V1 free software license agreement.

The validation of the CALIF^{3}S-P^{2}REMICS software is performed against a wide range of experiments. A part of this validation work is presented in this paper, namely the deflagration simulation of a large scale turbulent underexpanded hydrogen jet.

This paper is structured as follows. After a detailed description of the physical models (Section 2.0) and an overview of the numerical schemes (Section 3.0) used in the simulations, the underexpanded hydrogen jet deflagration scenario (Section 4.1) is presented. Then, the numerical results obtained for the dispersion phase (Section 4.3) and for the combustion phase (Section 4.4) are detailed.

2.0 THE CALIF^{3}S-P^{2}REMICS PHYSICAL MODELS

The dispersion of explosive gases and their deflagration take the form of turbulent flows. These flows are either (quasi)incompressible (*i*.e. governed by the asymptotic model derived in the limit of vanishing Mach number flows) or compressible. The turbulent transfers of temperature and chemical species generate large space and time variations of the density, up to obtain in some situations buoyancy driven flows (out of the validity range of the Boussinesq approximation). Most of dispersion applications fall in this category. After the onset of chemical reactions, the flow is essentially governed by the progression of the flame brush in the explosive atmosphere. In the deflagration and in the detonation case, the thickness of the flame brush turns out to be several orders of magnitude smaller than the characteristic size of the computational domain. Thus, the reaction zone needs to be described by specific models, obtained at least through a multi-scale approach, or, better, via multi-level techniques. In the present version of the software, this complex physics is dealt with by a turbulent flame velocity model. So, the problem boils down to the prediction of a single parameter, the flame brush velocity, as a function of the local turbulence and composition of the flow. This modelling will be complemented in a near future by more predictive approaches, coupling Large Eddy Simulation (LES) techniques with the derivation of a reaction rate based on upscaling techniques. The CALIF^{3}S-P^{2}REMICS software also features some diphasic models, to describe the steam condensation on walls and the transport by the flow of a diphasic dispersed phase (usually, water droplets), exchanging mass, momentum and energy with the carrier phase. In this latter case, the dispersed phase is decribed by a Lagrange approach (so yielding a Lagrange/Euler model for the whole flow).

The presentation of the model is restricted here to the useful part for the simulations presented in this paper. In the next section (Section 2.1), a comprehensive list of the involved balance equations is given, then the closure laws for the turbulent momentum, heat and mass transfers (Section 2.2) are detailed.

2.1 Balance Equations

The system of equations governing the flow – The hydrodynamics of the flow obey the compressible Navier-Stokes equations:

$$\partial_t(\rho) + \mathrm{div}(\rho\,\boldsymbol{u}) = 0, \qquad \partial_t(\rho\,\boldsymbol{u}) + \mathrm{div}(\rho\,\boldsymbol{u}\otimes\boldsymbol{u}) + \boldsymbol{\nabla} p - \mathrm{div}\boldsymbol{\tau} = \rho\,\boldsymbol{f}, \tag{1}$$

where ρ, $\boldsymbol{u}$, p, $\boldsymbol{\tau}$ and $\boldsymbol{f}$ stand for the density, the velocity, the pressure, the viscous stress tensor and a forcing term, respectively (usually, $\boldsymbol{f}$ stands for gravity forces, when they are taken into account, which is not the case in the present study). The considered energy balance equation is the so-called sensible enthalpy balance equation, which reads:

$$\partial_t(\rho\,h_s) + \mathrm{div}(\rho\,h_s\,\boldsymbol{u}) + \sum_{i=1}^{N_s} \mathrm{div}(h_{s,i}\,\boldsymbol{j}_i) - \partial_t p - \boldsymbol{u}\cdot\boldsymbol{\nabla} p - \mathrm{div}(\lambda\boldsymbol{\nabla}\theta) = \dot{\omega}_\theta + \boldsymbol{\tau}(\boldsymbol{u}) : \boldsymbol{\nabla}\boldsymbol{u} + \dot{Q}, \tag{2}$$

with h_s the mixture sensible enthalpy, $h_{s,i}$ the sensible enthalpy of the i^{th} chemical species, λ the turbulent heat diffusion coefficient, θ the temperature and $\dot{Q}$ the heat source term (including a possible external production and the effects of radiative heat transfers), neglected for this study. The heat production rate due to the chemical reaction, $\dot{\omega}_\theta$, is given by $\dot{\omega}_\theta = -\sum_{i=1}^{N_s} \Delta h^0_{f,i}\,\dot{\omega}_i$, where N_s is the number of considered chemical species in the flow, $\Delta h^0_{f,i}$ is the formation enthalpy of the i^{th} chemical species and $\dot{\omega}_i$ stands for the reaction rate of the species i. The mixture and chemical species enthalpies and the temperature are linked by $h_s = \sum_{i=1}^{N_s} y_i\,h_{s,i}$, and $h_{s,i} = c_{\mathrm{p},i}\,\theta$, for $1 \le i \le N_s$, where $c_{\mathrm{p},i}$ and y_i stand respectively for the specific heat and the mass fraction of the i^{th} chemical species. Finally, the atmosphere is supposed to be a mixture of perfect gases, *i*.e. the system is closed by the following equation of state:

$$p = \rho\,\frac{R}{W}\,\theta, \tag{3}$$

where W is the mixture molar mass and R stands for the perfect gas constant.

A wide range of RANS models ("high-Reynolds" variants, with the usual wall laws, and low-Reynolds models), together with Large Eddy Simulation models are available to describe turbulence. In the present studies, the so-called $k-\epsilon$ model (with k the kinetic energy associated to velocity fluctuations and ϵ the turbulent dissipation rate) is used. With the Boussinesq assumption, turbulence effects are modelled by additional diffusion fluxes, which are given in Section 2.2 below.

In some particular situations, the flow presents the following features: the velocity is low with respect to the speed of sound and the phenomena of interest are governed by convective and diffusive transfers. The phenomena occur at a time scale much greater than acoustic pressure fluctuations. In such a case, it is valuable from a numerical point of view to use a modified formulation of the Navier-Stokes equations, designed to filter out the acoustic waves. This model is referred to in the literature as the asymptotic model for low Mach number flows [3]. It is obtained from the presented compressible model by slight modifications:

- the pressure p in the equation of state is replaced by a quantity P_{th} called the thermodynamic pressure, which is constant in space. The time variations of P_{th} in a closed domain may be deduced from the overall conservation of mass and volume. If the domain is open, P_{th} is constant in time also.
- the pressure advection (*i*.e. the term $\boldsymbol{u}\cdot\boldsymbol{\nabla}p$) and the viscous dissipation (*i*.e. the term $\boldsymbol{\tau}(\boldsymbol{u}):\boldsymbol{\nabla}\boldsymbol{u}$) at the left-hand side and right-hand side, respectively, of the enthalpy balance (2) are disregarded, and the pressure time-derivative $\partial_t p$ is replaced by the time derivative of the thermodynamical pressure.

The low Mach number model is used in this paper for the dispersion phenomena simulation (Section 4.3) while the compressible model is used for the deflagration phase simulation (Section 4.4).

Modelling the chemical reactions – The turbulent deflagrations modelling in CALIF^{3}S-P^{2}REMICS is based on a *turbulent flame-speed closure* approach. The flame brush location is determined by a phase-field-like technique, solving a transport equation for a characteristic function (more precisely speaking, a *Hamilton-Jacobi* equation), leading to a formulation which is reminiscent of the so-called G-equation based models [4]. The unknown of this transport equation is thus denoted here by G and referred to hereafter as the "G-field". It obeys the following relation:

$$\partial_t(\rho G) + \mathrm{div}(\rho G\boldsymbol{u}) + \rho_u u_f|\boldsymbol{\nabla}G| = 0, \tag{4}$$

where the quantity ρ_u stands for the unburnt gases density, computed with the equation of state from fresh temperature and composition, and u_f is the turbulent flame velocity. Flame ignition is obtained by setting $G = 0$ in a small neighbourhood of the ignition point and $G = 1$ elsewhere (so, thanks to the mathematical properties of Equation (4), G remains in the interval $[0, 1]$ throughout the simulations). The classical reactive formulation of the chemical species mass balance equations is keeped to cope with partially premixed situations. The reaction term is evaluated as a function of G: it is set to zero in the fresh zone ($G \geq 0.5$), and to a finite (but possibly large) value in the burnt zone ($G < 0.5$). Only four gaseous chemical species are supposed to be present in the flow, namely the fuel (denoted by F), the oxydant (O), the products (P) of the reaction, and a neutral gas (N). A one-step irreversible total chemical reaction is considered:

$$\nu_F F + \nu_O O + N \rightarrow \nu_P P + N,$$

where ν_F, ν_O and ν_P are the molar stoichiometric coefficients of the reaction. The system of the mass balance equations for the chemical species reads:

$$\partial_t(\rho y_i) + \mathrm{div}(\rho y_i\boldsymbol{u}) + \mathrm{div}(\boldsymbol{j}_i) = \dot{\omega}_i, \qquad \text{for } 1 \leq i \leq N_s, \tag{5}$$

where $\boldsymbol{j}_i$ stands for the (turbulent) mass diffusion flux of the species i. Switching from the notation $(y_i)_{1\leq i\leq N_s}$ to y_F, y_0, y_P and y_N for the fuel, oxydant, product and neutral gas mass fractions, respectively, the reaction rate of each chemical species may be written as $\dot{\omega}_F = -\nu_F W_F\,\dot{\omega}$, $\dot{\omega}_O = -\nu_O W_0\,\dot{\omega}$, $\dot{\omega}_P =$

$\nu_P W_P\,\dot{\omega}$ and $\dot{\omega}_N = 0$, where W_F, W_0 and W_P stand for the molar masses of the fuel, oxydant and product respectively, and $\dot{\omega}$ is a non-negative reaction rate, which is supposed to vanish when either $y_F = 0$ or $y_O = 0$ and, as announced, is governed by the value of G:

$$\dot{\omega} = \frac{u_f}{\delta}\,\eta(y_F, y_O)\,(G - 0.5)^-, \quad \eta(y_F, y_O) = \min(\frac{y_F}{\nu_F W_F}, \frac{y_O}{\nu_O W_O}), \tag{6}$$

where for $a \in \mathbb{R}$, $a^- = -\min(a, 0)$ and δ is a quantity homogeneous to a length scale, which governs the thickness of the reaction zone. Although this quantity could possibly be evaluated by physically grounded arguments, here the assumption that the thickness of the flame brush is small compared to the observation scale is made. Thus δ is set to an arbitrarily small value and the combustion is (almost) instantaneous.

Finally, the model is closed by a turbulent flame speed correlation, the most frequently encountered in the literature are available in P^{2}REMICS. These correlations allow to compute u_f as a function of the local turbulence and as a function of the laminar flame speed, which depends on the local temperature and pressure and on the local mixture composition.

2.2 Expression of the Turbulent Diffusion Fluxes

The turbulent viscous stress tensor is given by:

$$\boldsymbol{\tau} = \mu_t\,(\boldsymbol{\nabla u} + \boldsymbol{\nabla}^t \boldsymbol{u}) - \frac{1}{3}\mu_t\,\mathrm{div}(\boldsymbol{u})\,\boldsymbol{I} - \frac{2}{3}\,k\,\boldsymbol{I},$$

where the apparent viscosity μ_t stands for the turbulent viscosity and $\boldsymbol{I}$ stands for the identity matrix. In the present work, the term $\mathrm{div}(-2/3\,k\,\boldsymbol{I}) = -2/3\,\boldsymbol{\nabla} k$ may be neglected in front of $\boldsymbol{\nabla} p$, so it is set to zero in practice. In the framework of RANS modelling of turbulent flows, it is often assumed that the (turbulent) Prandtl number Pr is constant and takes a value close to 1, and that the Lewis number Le is equal to 1. Once the turbulent viscosity μ_t given by the turbulence model, the thermal conductivity could be written as:

$$\lambda = \frac{\mu_t\,c_\mathrm{p}}{\mathrm{Pr}} = \frac{\mu_t}{\mathrm{Pr}}\sum_{i=1}^{N_s} c_{\mathrm{p},i}\,y_i. \tag{7}$$

The mass fluxes of the chemical species are given by:

$$\text{for } 1 \le i \le N_s, \quad \boldsymbol{j}_i = -\rho\,D_i\,\boldsymbol{\nabla} y_i = -\frac{\mu_t}{\mathrm{Pr}}\,\boldsymbol{\nabla} y_i. \tag{8}$$

In addition, the assumption that Le = 1 allows giving another form for some terms of the enthapy balance equation:

$$-\frac{\mu_t}{\mathrm{Pr}}\boldsymbol{\nabla} h_s = -\frac{\mu_t}{\mathrm{Pr}}\,c_\mathrm{p}\boldsymbol{\nabla}\theta - \frac{\mu_t}{\mathrm{Pr}}\,\theta\,\boldsymbol{\nabla} c_\mathrm{p} = -\underbrace{\frac{\mu_t}{\mathrm{Pr}}\,c_\mathrm{p}}_{\lambda}\,\boldsymbol{\nabla}\theta + \sum_{i=1}^{N_s} c_{\mathrm{p},i}\,\theta\,\underbrace{(\mu_t/\mathrm{Pr})\boldsymbol{\nabla} y_i}_{\boldsymbol{j}_i}.$$

Hence, the enthalpy balance (2) may be recasted as:

$$\partial_t(\rho\,h_s) + \mathrm{div}(\rho\,h_s\,\boldsymbol{u}) - \mathrm{div}(\frac{\mu_t}{\mathrm{Pr}}\,\boldsymbol{\nabla} h_s) - \partial_t p - \boldsymbol{u}\cdot\boldsymbol{\nabla} p = \dot{\omega}_\theta + \boldsymbol{\tau}(\boldsymbol{u}) : \boldsymbol{\nabla}\boldsymbol{u}, \tag{9}$$

which is indeed done in CALIF^{3}S-P^{2}REMICS.

3.0 OVERVIEW OF CALIF^{3}S-P^{2}REMICS (or CALIF^{3}S) NUMERICS

The CALIF^{3}S [2] provides solvers for a rather comprehensive set of Partial Differential Equations of fluid dynamics: Navier-Stokes equations, balance equations for mass (overall mass balance or chemical species mass balance), energy balance, equations of statistical (RANS) models for turbulence... The time discretization implements an (essentially first order in time) fractional step strategy, consisting in solving successively equations or blocks of equations. Among these blocks, a notable one is the Navier-Stokes equations (*i*.e. mass and momentum balance for (quasi-)incompressible flows and mass, momentum and energy balances for compressible flows). Navier-Stokes equations are treated in a specific way, usually by a pressure correction technique. An explicit solver, dedicated to (almost) inviscid compressible flows (*i*.e. Euler equations for detonation or blast wave applications and LES of compressible flows), is also available.

The space discretization is staggered type one: scalar variables, and their governing equations, are associated to cells while velocity components are associated to faces (or, in other words, to a dual mesh). This kind of discretizations are natively stable for incompressible flows, in the sense that no corrective action (typically perturbations of the mass balance) has to be implemented to avoid the pressure odd-even decoupling observed with collocated schemes (*i*.e. schemes where both pressure and velocity components are associated to the cells). In counterpart, the implementation of such a discretization for compressible flows needed the development of new schemes, performed in collaboration with IRSN and the Aix-Marseille University (see e.g. [5, 6] for recent papers). Obtained schemes have been shown to satisfy the same stability properties (preservation of natural physical properties as positivity of the density, the pressure and the internal energy and entropy estimates) as collocated ones, while using very simple fluxes well suited to intensive computing. Indeed, stability results from a simple upwinding with respect to the material velocity, thus avoiding the burden of any exact or approximate solution of Riemann problems at each face. In addition, these schemes are accurate uniformly with respect to the Mach number, this point has deserved a literature running over the last decades. Last but not least, the CALIF^{3}S library is based on homogeneous space discretizations, which saves implementation efforts and facilitates the chaining of different solvers, as performed in the validation test presented hereafter.

The CALIF^{3}S library deals with unstructured (quadrangles/hexahedra or simplices) meshes, and with non-conforming local refinement. In any case, a particular care has been spent to preserve stability properties, as the preservation at the discrete level of maximum principles enjoyed by transport operators (for instance, ensure the density positivity or, for non-reactive flows, keep the chemical species mass fractions in the same interval as initial and boundary conditions). The schemes used in applications are usually of second order in space.

Parallelism relies on a domain decomposition approach, with the notable exception of radiative intensity steady transport equations, which are distributed among the processors (a processor deals with some equations posed over the whole mesh, potentially coarsened to save memory and computation time). CALIF^{3}S proposes distributed linear solvers (essentially Krylov solvers), either from extern libraries as PETSc or, for the more frequently algorithms, from CALIF^{3}S itself (in this latter case, with equivalent performances).

4.0 DEFLAGRATION IN AN UNDEREXPANDED JET

4.1 Experimental Procedure

The considered experiment is led at INERIS, with a dedicated experimental device [7], consisting in a pressurized tank containing hydrogen, provided with an ejection pipe. The release generates a large scale horizontal jet (more than 10 m long) in an open atmosphere. The reservoir has a storage volume of 5 m^3 and an initial pressure of 40 bars. The release diameter is 12 mm allowing for a quasi-constant release

mass flow rate during the first 20 s. The release point is located at 1.5 m above the floor. The experiment is performed in two steps:

- a dispersion phase: un-ignited gas release is carried out, up to obtain a steady jet,
- a combustion phase: delayed explosion of this gas release is performed at 1.8 m from the nozzle (corresponding to an hydrogen volume concentration of 30%).

The ignition occurs 5 s after the start of the hydrogen release.

4.2 Numerics

Numerical simulations follow the same two steps as the experimental procedure. First the free jet is characterized before ignition, then the dispersion phase results are used as initial conditions for the explosion simulation. The computations of the dispersion and deflagration phases are performed with the same computational domain and meshing. The simulations are performed on a 2D axisymmetrical computational domain instead of a 3D domain to allow faster computations (so disregarding the effects of the gravity on the jet shape, and then the reflection of the pressure waves on the ground). The symmetry axis is the ordinate axis (so computational results are drawn as if the jet was vertical). The domain is chosen large enough to avoid the reflexion on the boundary of the pressure waves generated by the deflagration. The mesh is composed of embedded structured grids, with square cells. At each mesh-level transition, the space step is divided by two (so each cell is subdivised in four), the finest meshes being located near the injection. The minimum (resp. maximum) length of the cells edges is close to 0.35 cm (resp. 2.4 cm). The total number of cells is close to $5\,10^5$. The time step is computed in order to have a Courant-Friedrichs-Lewy condition $CFL = 80$ for the dispersion phase and $CFL = 0.2$ for the combustion phase, with respect to the velocity at the nozzle.

4.3 Dispersion Phase

For the dispersion phase simulation, a difficulty lies in the modelling of the vicinity of the hydrogen release. Indeed, the hydrogen flows out in critical conditions, with a pressure at the nozzle higher than the ambiant pressure and, over a distance of some nozzle diameters, compressible effects are predominant and generate a complex structure of shock waves. In addition, the space and time scales of compressible phenomena are small compared to the characteristic scales of the flow: they take place in a zone of 20-30 diameters long, so, here $20 - 30$ cm, while the size of the whole jet is about 10 m. Shock structures are established in a few milliseconds while the steady state of the jet is reached in some tens of seconds. To circumvent this problem, the inlet conditions are replaced by fictitious ones, built to preserve the behaviour of the jet far from the release nozzle, while filtering out the compressible effects, in such a way that a quasi-incompressible model may be used. This artificial boundary condition is referred as a "notional nozzle" approach [8, 9, 10, 11]. Three different notional nozzle approaches are compared hereafter, namely the Birch model [9], the Ewan and Moodie model [10] and the correlation used in the FLACS software [11]. Turbulence is modelled by the standard $k - \epsilon$ model.

The numerical results are compared with the experimental data and with some literature correlations, relying on self-similarity assumptions, which are given hereafter. The centreline mass fraction decays are reported on Fig. 1. The fuel concentration decreases rapidly, by turbulent diffusion of the ambient air into the jet. The centreline mass fraction decay for nonreacting jets can be correlated with the distance from the virtual origin x_o of the jet by [12]:

$$Y_F(0, z) = \frac{K_c\, D_{eff}}{x - x_o}$$

where D_{eff} is referred to as the effective diameter and the parameters $K_c = 4.8$ and $x_o = 4\,d$, with d the nozzle diameter, are two constants. The Ewan and Moodie or the Birch models yield results which are

closer to the experimental data than those obtained with the FLACS approach, which overestimates the fuel concentration. In addition, as already pointed out in [8], the Birch model seems to perform better than the Ewan and Moodie one.

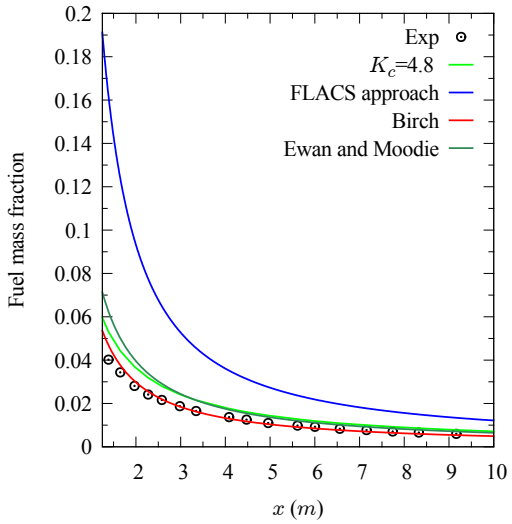

Figure 1. Fuel mass fraction along the axis

The radial profiles of fuel mass fractions are plotted in Fig. 2 as a function of jet similarity variables (*i*.e. the mean mass fraction is normalized by the centreline value and the radial distance by the distance from the origin). The numerical results obtained with the Birch and the Ewan and Moodie models show a good agreement with the experimental data and with the previous correlation, whereas the FLACS correlation yields slightly lower relative mass fractions (which is a direct consequence of the fact that the radial diffusion is underestimated). In addition, it is observed that, as in standard (*i*.e. incompressible) inertia-driven jets, the normalized mass fraction and the distance from the virtual origin can be correlated by [13]:

$$\frac{Y_F(r,z)}{Y_F(0,z)} = \exp\left\{-K_r\left(\frac{r}{x-x_o}\right)^2\right\}$$

where r is the distance to the jet axis and K_r is a constant taken to 34.6 for these experiments [7].

Concerning velocity profiles, similar conclusions can be drawn. In addition, our results are in close agreement with computations performed by other authors [13, 14], and, here also, the Ewan and Moodie model still gives the better results. The experimental data show that the relative turbulence intensity (standard deviation) is in the range from 15% to 30% [13] and exponentially increases with the normalized radial distance r/x [7] (Fig. 3). Similar observations can be made for the standard deviations obtained numerically, regardless of the notional approach used. The results obtained with the Ewan and Moodie model are reported on Fig. 3.

4.4 Combustion phase

For the simulation of the deflagration, a fully compressible formulation is used for hydrodynamics. Various correlations for the turbulent burning velocity can be found in the literature. The Bradley's correlation [15], the Bray's correlation [16], the Zimont correlation [17] and the Peters correlation [4, 18] are compared here. These closure laws yield the turbulent flame velocity as a function of the local turbulence and of the laminar flame velocity. This latter, given itself by the correlation introduced in [19], depends on the local atmosphere composition, and thus varies with time and space in partially premixed situations as encountered here. The deflagration is simply initiated by setting 0 as initial value for the

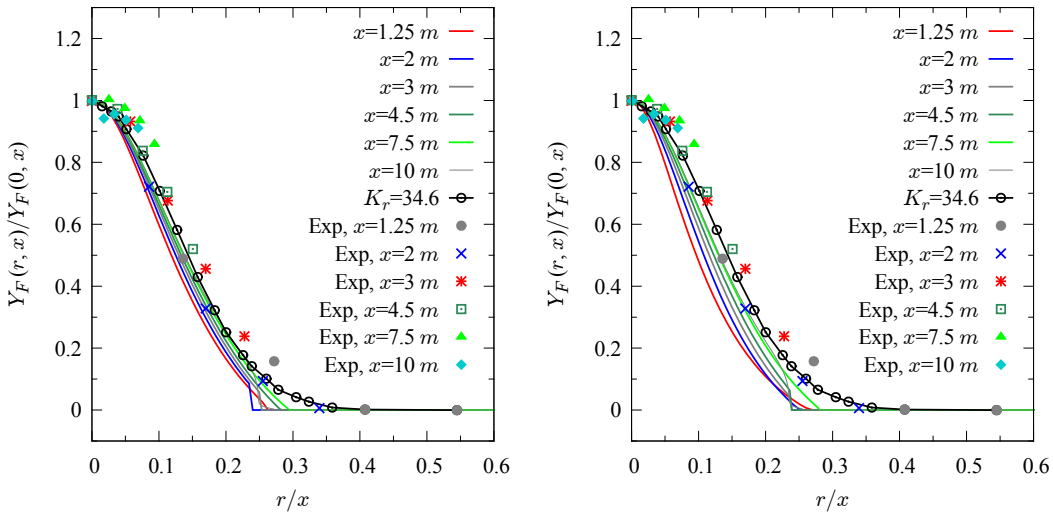

Figure 2. Normalized mass concentration along the normalized radius – Left: Birch approach. Right: FLACS model

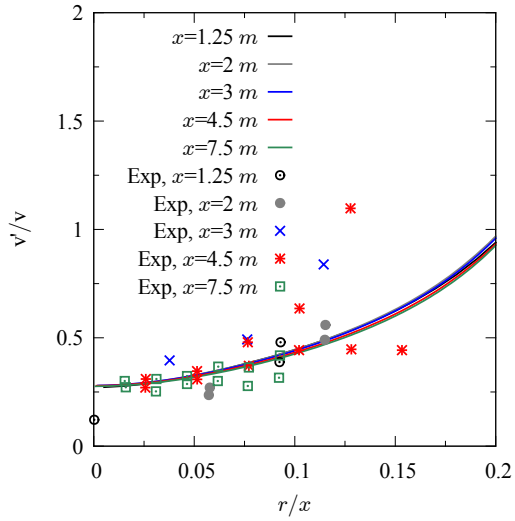

Figure 3. Standard deviation along the normalized radius (Ewan and Moodie approach)

G-field in the vicinity of the ignition point. Turbulence is modelled by the $k-\epsilon$ model with the Kato and Launder [20] modification to prevent from excessive dissipation in compression/expansion zones. The numerical results obtained with the Ewan and Moodie model for the dispersion phase are chosen as initial conditions for the explosion phase.

Structure of the flow – Let us first recall the flow structure in the case of a spherical deflagration in a perfectly premixed atmosphere. Supposing that the diffusion phenomena may be neglected and that the infinitely-thin flame brush moves with a constant velocity, solutions for this model problem may be found in the literature [21, 22]. The flow is separated in three distinct zones, limited by spherical interfaces:

- From the ignition point to the outside atmosphere, a central burnt zone is first encountered, where the flow is at rest, and the pressure and temperature are constant, and higher than initially.
- This burnt zone is delimited by the flame brush, where flow characteristic variables jump: from the inner to the outer side, the pressure and the radial velocity increase. Crossing the flame brush, an intermediate zone is encountered, where the composition of the gas is the initial fresh composition, and gases are pushed outward by the expansion of the burnt gases. Along the radius, the pressure,

velocity and density decrease because of the spherical geometry (it would be constant for a 1D plane flame brush), while the entropy is constant. On its outer side, this zone is delimited by a shock, referred to as the *precursor shock*.

- Finally, at the exterior side of the precursor shock, the initial flow state is found (fluid at rest, initial pressure, temperature and composition).

For the problem at hand, some deviations from this ideal situation may be anticipated, because the fluid is not initially at rest and its composition strongly varies (the fuel is essentially located near the jet centerline, and its concentration decreases along the jet). This composition effects can be investigated thanks to a 1D model problem (not showed here because of a lack of space), where it is observed that:

- first, the symmetry is broken because the variable composition yields a variable-in-space equation of state, and thus variable-in-space Rankine-Hugoniot jump conditions,
- more importantly, the variations in space of the combustion energy generate strong velocities in the burnt zone. In particular, when combustion stops on "one side" of the burnt zone, burnt gases are pushed away in this direction.

Fig. 4 shows some pressure and G-field isovalues. In all the pictures, the expected two pressure waves are observed: from the ignition point, the reactive shock is first encountered (at the flame front location), then the precursor shock. In the first two pictures, a small-magnitude pressure wave is generated near the nozzle and gradually disappears. This phenomenon is purely numerical and is due to the change of solver between the incompressible dispersion computation (used as initial value for the explosion phase) and the compressible one. Still as expected because of the non-homogeneity of concentrations, in all the pictures of Fig. 4, the pressure waves are not symmetrical in the radial and in the axial directions and their structure changes with time. The magnitude of the overpressure generated at the flame brush decreases as the flame front moves forward the jet (as the initial fuel concentration decreases too). In the third picture, the flame front enters, on its farthest side from the axis, into a zone with no fuel and a new pressure wave, namely a rarefaction wave moving to the right, appears.

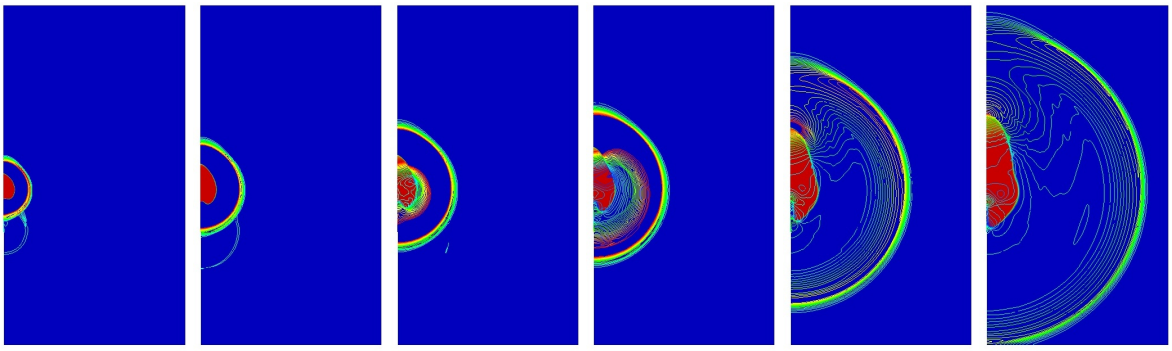

Figure 4. G-field and pressure isovalues (from 9.8×10^4 Pa to 1.05×10^5 Pa), for $t = 3$ m to $t = 9$ m with a step of 2 ms, and at $t = 15$ ms and $t = 20$ ms

On Fig. 5 (left), the pressure and velocity fields (with a constant length for velocity vectors, independently of the norm of the velocity) are presented at a given time of the transient. As in the previous figure, the reactive and the precursor shocks can be observed. In addition, along the jet centerline before (respectively after) the flame brush, a strong fluid motion is observed in direction of the nozzle (respectively in the same direction as the jet). This is due to the fact that the chemical reaction essentially happens on the farthest side of the flame brush with respect to the nozzle. As expected from the above-mentionned 1D model problem, the sudden gas expansion generates a flow issued from the reaction zone and perpendicular to the flame surface. These counter-current and co-current (with respect to the jet direction) flows are of strong magnitude: velocities are in the range of 200 m/s, and thus much greater than the flame speed itself ($\simeq$ 15 m/s with respect to the fresh gases flow). Near the nozzle, the counter-current flow comes to interact with the inlet hydrogen jet. This flow structure remains the same

throughout the flame propagation. Outside the surface delimitated by the precursor shock, as expected, the undisturbed state is obtained, *i*.e. the fluid is at rest (in this area, the fact that all the velocity vectors have the same length is misleading) and at the atmospheric temperature and pressure.

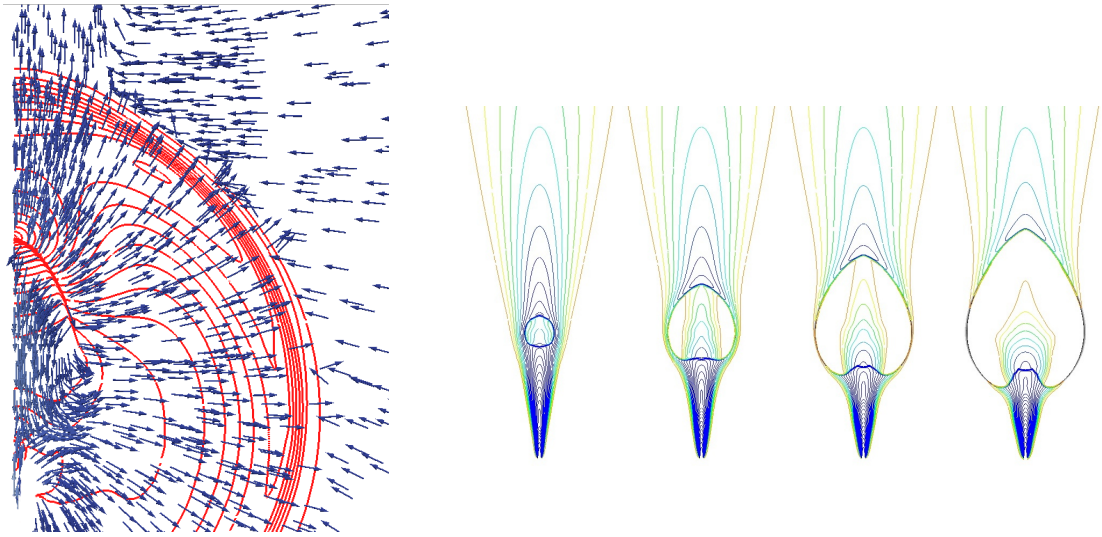

Figure 5. Left: pressure isovalues and normalized velocity vectors. Right: isovalues of the hydrogen molar fraction and G-field from $t = 1$ ms to $t = 7$ ms with a step of 2 ms

On Fig. 5 (right) the hydrogen molar fraction and G-field isovalues are plotted. The thicker line shows the flame front position. As the flame front propagates, two zones appear in the burnt phase: near the jet axis and near the nozzle, the air/hydrogen mixture (at least at the time of observation) is over-stoichiometric. Farther from the axis or inlet section, the fuel mass fraction vanishes and the oxydant is in excess (*i*.e. lean region). Above the burned zone, the fuel is pushed by the flame front, but its mass fraction field keeps the same structure. Near the nozzle, some fuel is injected by the jet inside the burnt zone, but the above-mentionned countercurrent flow prevents its progression in the axial direction.

Pressure signals – In the deflagration phase, the overpressure is measured by three piezoresistive Kistler pressure sensors [7]. Here, only the results obtained for sensors located respectively on the axis of the jet downstream from the igniter, at 2 m and at 2.5 m of the ignition point, in the perpendicular direction to the jet axis will be shown. These sensors are referred respectively to as the L2 and the L3 sensor. All the experiments have been performed twice in order to check the measurements accuracy.

The overpressures at the L2 and L3 measurement points, obtained with the Peters turbulent burning velocity correlation are compared to experimental data on Fig. 6. The greatest experimental overpressure is measured 2 m downstream from the igniter (L2 sensor). The maximum overpressure is approximatively 60 mbar and is reached around 10 m from ignition. The L3 sensor measures a pressure level similar to that obtained with the L2 sensor. However, the pressure peak is lower: the fuel concentration quickly decreases in the radial direction, and the combustion stops. A second pressure peak seems to appear in the experimental pressure. It may be due to the reflection of the precursor shock on the ground, which cannot be computed by the code (indeed for axisymmetrical modelling the floor is not represented). After this second peak, the recorded overpressure becomes negative, but this is probably due to a failure of the sensor. The numerical results obtained with the Peters correlations show the same tendency as experiment overpressure signals. The slope of the pressure evolution for the L2 gauge is however steeper than the experimental one and the overpressure peak is encountered later for the L3 gauge, so the predicted flame speed is slightly higher than the experimental one. The reached overpressure is close to the experimental one for all the pressure gauges. In Fig. 6, the oscillations at the level of the second pressure peak seem to be due to the interaction between the jet and the flame brush when this latter is close to the nozzle. Conversely, the overpressures obtained by CALIF^{3}S-P^{2}REMICS with the Bray, Bradley and Zimont turbulent burning velocity correlations are much higher (up to a factor 10) than the experimental

ones. Such a large dispersion of results had already been quoted for simpler flows [23].

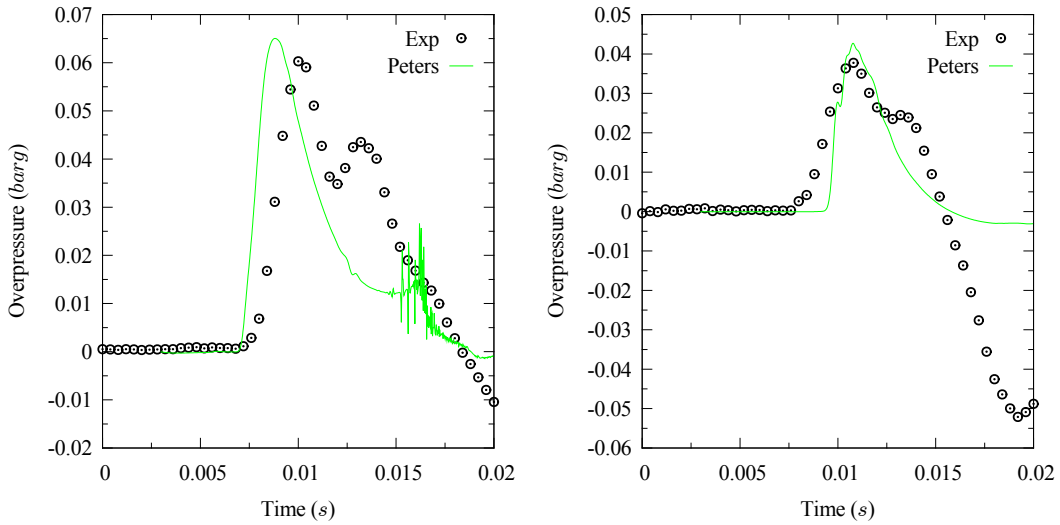

Figure 6. Overpressure evolution at L2 (left) and L3 (right) sensors with v_f computed with the Peters flame speed correlation

5.0 CONCLUSION

In this paper, the establishment of a large scale underexpanded hydrogen flow in an open atmosphere and its deflagration have been simulated with the CALIF^{3}S-P^{2}REMICS software. The jet deflagration is described by a turbulent flame speed closure model. Generally speaking, numerical results are in reasonable agreement with the experimental ones. However, for the description of the deflagration, some dispersion is obtained when testing different, but well established in the literature, turbulent flame speed correlations. In order to obtain more predictive simulations, it seems that (at least) the following issues should be addressed:

- complete the model assessment to obtain a more comprehensive validation basis,
- perform experiments with an as accurate as possible characterization of the turbulence in the fresh atmosphere, ahead of the flame brush,
- comfort the present modelling by comparison to a more sophisticated approach, based on Large Eddy Simulation techniques.

All these tasks are ongoing, the first and the third one are currently in progress in the framework of the CALIF^{3}S-P^{2}REMICS project. Turbulence measurements are planned in the flame acceleration large-scale ENACCEF 2 facility, operated with the support of IRSN in the ICARE laboratory of the French Centre National de la Recherche Scientifique (CNRS, Orléans).

REFERENCES

1. P^{2}REMICS, Collaborative development environment, IRSN, https://gforge.irsn.fr/gf/project/p2remics.
2. CALIF^{3}S. Collaborative development environment, IRSN, https://gforge.irsn.fr/gf/project/calif3s.
3. Majda, A., Sethian, J., The derivation and mumerical solution of the equations for zero Mach number combustion, *Combustion Science and Techniques*, **42**, 1985, pp. 185–205.
4. Peters, N., Turbulent combustion, 2000, Cambridge University Press, Cambridge Monographs of Mechanics.

5. Grapsas, D., Herbin, R., Kheriji, W., Latché, J.-C., An unconditionally stable staggered pressure correction scheme for the compressible Navier-Stokes equations, *SMAI Journal of Computational Mathematics*, **2**, 2016, pp. 51–97.

6. Gastaldo, L., Herbin, R., Latché, J.-C., Therme, N., A MUSCL-type segregated–explicit staggered scheme for the Euler equations, *Computers & Fluids*, **175**, 2018, pp. 91–110.

7. Daubech, J., Hebrard, J., Jallais, S., Vyazmina, E., Jamais, D., Verbecke, F., Un-ignited and ignited high pressure hydrogen releases: concentration–turbulence mapping and overpressure effects, *Journal of Loss Prevention in the Process Industries*, **36**, 2015, pp. 439–446.

8. Papanikolaou, E., Baraldi, D., Kuznetsov, M., Veenetsanos, A., Evaluation of notional nozzle approaches for CFD simulations of free-shear under-expanded hydrogen jets, *International Journal of Hydrogen Energy*, **37**, 2012, pp. 18563–18574.

9. Birch, A.D., Hugues, D.J., Swaffield, F., Velocity decay of high pressure jets, *Combustion Science and Technology*, **52**, 1986, pp. 161–171.

10. Ewan, B.C.R., Moodie, K., Structure and velocity measurements in underexpanded jets, *Combustion Science and Technology*, **45**, 1986, pp. 275–288.

11. FLACS v9.0 User's Manual, Gexcon Technical report.

12. Scheffer, R.W., Houf, W.G., Williams, T.C., Investigation of small-scale unintended releases of hydrogen: momentum-dominated regime, *International Journal of Hydrogen Energy*, **33**, 2008, pp. 6373–6384.

13. J. O. Hinze, Turbulence, 1975, McGraw-Hill.

14. Chen, C.J., Rodi, W., Vertical turbulent buoyant jets, *Pergamon press* 1980.

15. Bradley, D., Lau, A.K.C., Lawes, M., Flame stretch rate as a determinant of turbulent burning velocity, *Philosophical Transactions of the Royal Society of London A*, **338**, 1992, pp. 359–387.

16. Bray, K.N.C., Studies of the turbulent burning velocity, *Proceedings of the Royal Society of London A*, **431**, 1990, pp. 315–335.

17. Zimont, V.L., Gas premixed combustion at high turbulence. Turbulent flame closure combustion model, *Experimental Thermal and Fluid Science*, **21**, 2000, pp 179–186.

18. Wirth, M., Peters, N., Turbulent premixed combustion : a flamelet formulation and spectral analysis in theory and IC-engine experiments, 24th Symposium (International) on Combustion - The Combustion Institute, 1992, pp 483–501.

19. Iijima, T., Takeno, T., Effects of temperature and pressure on burning velocity, *Combustion and Flame*, **65**, 1986, pp. 35–43.

20. Kato, M., Launder, B.E., The modeling of turbulent flow around stationary and vibrating square cylinders, 9th Symposium on Turbulent Shear Flows, 1993, pp. 1041–1046.

21. Sedov, L.I., Similarity and dimensional methods in mechanics, *CRC Press* 2000.

22. Grapsas, D., Herbin, R., Latché, J.-C., Nasseri, Y., Modelling of a spherical deflagration at constant speed, *submitted* 2019.

23. Dahoe, A. E., Skjold, T., Roeckaerts, D.J.E.M., Pasman, H.J., Eckhoff, R.K., Hanjalic, K., Donze, M., On the application of the Levenberg-Marquardt method in conjunction with an explicit Runge Kutta and an implicit Rosenbrock method to assess burning velocities from confined deflagrations, *Flow, Turbulence and Combustion*, **91**, 2013, pp. 281–317.